Role of the *Campylobacter jejuni cheVAWY* chemotaxis genes in chemotactic motility and biofilm formation

Mark Reuter[1], Eveline Ultee[1], Yasmin Toseafa[1], Andrew Tan[1], and Arnoud H.M. van Vliet[1,2,*]

1. Quadram Institute Bioscience, Gut Health and Food Safety Programme, Norwich Research Park, Norwich, United Kingdom.
2. University of Surrey, Department of Pathology and Infectious Diseases, School of Veterinary Medicine, Faculty of Health and Medical Sciences, Guildford, United Kingdom

* Address correspondence to Dr Arnoud van Vliet (a.vanvliet@surrey.ac.uk)

Running title: Chemotaxis and biofilm formation in *C. jejuni*

Keywords: Campylobacter, chemotaxis, biofilm formation, flagellar motility

Total number of words in Summary: 238

Total number of words in Manuscript text: 5,152

Number of Figures: 6, Number of Tables: 1

Supplementary information: 6 Figures, 2 Tables, 2 Movies (via Figshare)

Abbreviations: MCPs, methyl-accepting chemotaxis proteins; CheA-Y, receiver domain of CheA; M-MuLV, Moloney Murine Leukemia Virus; BAB, Blood Agar Base; PMT, photomultiplier tube.

ABSTRACT

Chemotaxis is the ability of motile bacteria to coordinate swimming behaviour to navigate a changeable environment, by sensing environmental conditions through receptors and transducing these signals to the flagellar motor. In the foodborne bacterial pathogen *Campylobacter jejuni*, flagellar motility and chemotaxis are required for intestinal colonisation and virulence. Here we present a systematic characterisation of the CheVAWY chemotaxis system of *C. jejuni* and its role in chemotactic motility and biofilm formation. Inactivation of the core chemotaxis genes (*cheA*, *cheY*, *cheV* or *cheW*) impaired chemotactic motility but not flagellar assembly. Inactivation of *cheV* or *cheW* or presence of two copies of *cheV* or *cheW* resulted in reduced chemotaxis. A *cheY* mutant swam in clockwise loops and this behaviour was complemented by wildtype *cheY* or a *cheY* gene lacking the D53 conserved phosphorylation site, but not by *cheY* lacking the D7 metal-binding site. Deletion of the CheY-like received domain from the *cheA* gene did not impair chemotactic motility, nor could this domain complement a *cheY* mutant. The *cj0350* gene was identified as encoding a putative CheX phosphatase, and the presence of two copies of *cj0350* resulted in reduced chemotactic motility. Finally, inactivation of any of the core chemotaxis genes interfered with the ability to form a discrete biofilm at an air-media interface. This work shows that interference with the *Campylobacter* chemotaxis system at any level disrupts optimal chemotactic motility, and also affects transmission modes such as biofilm formation and dispersal.

INTRODUCTION

Campylobacter jejuni is an important causative agent of bacterial gastroenteritis in humans [1], and is commonly transmitted via contaminated food, especially poultry meat [2]. Infection with *C. jejuni* is also associated with neurodegenerative diseases like Miller-Fisher and Guillain-Barre syndrome [3]. One of the key factors for infection by *C. jejuni* is its flagella-based motility, as aflagellated *C. jejuni* are unable to cause disease in animal models and show strongly reduced host cell invasion in cell culture-based assays [4-6]. The flagella are also involved in biofilm formation [7-9], and are targeted by bacteriophages [10].

Bacteria are able to adapt to changeable environments using a number of different strategies. Over time, genome plasticity and evolution allows for long-term adaptation to a particular niche. More immediate stresses are sensed by transcriptional regulators, resulting in changes in gene expression. By far the most rapid means of evading stress by motile bacteria is by changing swimming behaviour to escape unfavourable conditions or seek more favourable conditions, using chemotaxis to sense and move according to chemical gradients or intracellular signals [11]. The core chemotaxis pathway consists of the CheY-CheA two-component signal transduction system [12]. Stimulation of signal sensing methyl-accepting chemotaxis proteins (MCPs) results in autophosphorylation of the histidine kinase CheA, which transfers the phosphate group to the response regulator CheY. Phosphorylated CheY interacts with the flagellar switch to alter flagellar motor rotation. Counter-clockwise rotation commonly results in straight running motility while clockwise rotation results in a tumbling behaviour and directional change [13].

While the core CheA-CheY pathway is conserved in motile bacteria, the bacterial kingdom contains several variations on this theme [14, 15]. A number of accessory proteins can be involved, such as the CheW protein which is required for CheA-MCP interaction [16, 17], while a methyltransferase (CheR) and a methylesterase (CheB) modify the MCP proteins to accommodate adaptation [18]. Some organisms contain the CheW-like protein CheV, which may help integrate

signals from a specific class of sensors and may also act as a phosphate sink [19]. Phosphatases such as CheZ or CheX can dephosphorylate CheY to reduce its effect on flagellar rotation [20, 21]. Bacteria may also have multiple non-redundant homologs of the chemotaxis proteins or contain specific adaptations, adjuncts, and domain-fusions that add new functions to the core chemotaxis system [22].

Compared to other foodborne pathogens such as *E. coli*, *Salmonella*, and *Listeria*, *C. jejuni* has a greater number of MCPs involved in sensing amino acids, deoxycholate, dicarboxylic acid TCA intermediates, formic acid, fucose, redox, iron, phosphate and energy status [23-29], plus a core chemotaxis system consisting of CheVAWY proteins plus a CheR and a truncated CheB protein [4, 11], and the ChePQ regulatory system controlling the core chemotaxis genes *cheVAW* [30]. Chemotaxis-defective mutants have been shown to be attenuated in disease models [31-34], show reduced immunopathology [35] and chick colonization [34], and were reported to be crucial for infection in genome-wide transposon mutant screenings for virulence factors [36, 37].

In this manuscript we have used genetic inactivation, mutation and complementation to systematically examine the *cheVAWY* genes encoding the core chemotaxis pathway in *C. jejuni* (Fig. 1). We show that each signalling protein is necessary for chemotaxis in complex media, but not for motility. Furthermore, we show that the metal-binding site encoded by *cheY* is required for CheY function, but that the phosphorylation site is not required. Finally, we show that the receiver domain of CheA (CheA-Y) is dispensable for CheA function, but cannot complement a *cheY* mutant, and that chemotaxis is required for organized biofilm formation.

MATERIALS AND METHODS

C. jejuni strains and growth conditions.

Campylobacter jejuni strain NCTC 11168 and its isogenic mutants (Table 1) were routinely

cultured in a MACS-MG-1000 controlled atmosphere cabinet (Don Whitley Scientific) in microaerobic conditions (85% N_2, 5% O_2, 10% CO_2) at 37°C. For growth on plates, strains were either grown on Brucella agar or Blood Agar Base (BAB) with Skirrow supplement (10 μg ml^{-1} vancomycin, 5 μg ml^{-1} trimethoprim, 2.5 IU polymyxin-B). Broth culture was carried out in Brucella broth (Becton Dickinson).

Construction of insertional inactivation strains

Insertional inactivation mutants were made as described previously [26] using primers listed in Table S1, resulting in plasmids listed in Table S2. Plasmids were propagated in *E. coli* strain TOP10. To insert antibiotic resistance cassettes, *Bam*HI sites were introduced in the target genes by inverse PCR (Table S1) and ligated to either the kanamycin cassette from pMARKan9 (*ΔcheY*, Δ*cheW*, Δ*cheV*) or chloramphenicol cassette from pTopCat. All constructs were sequenced prior to transformation (Eurofins Genomics, Ebersberg, Germany). Single *C. jejuni* mutant strains were isolated after transformation of the *C. jejuni* NCTC 11168 wildtype strain with plasmids by electroporation [26], followed by selection on plates supplemented with either 50 μg ml^{-1} kanamycin or 10 μg ml^{-1} chloramphenicol. To confirm the position of the antibiotic cassette in antibiotic resistant clones, genomic DNA was isolated from four ml of overnight culture (DNeasy kit, QIAGEN). Diluted genomic DNA (50 ng) was used as template for PCR using primers that anneal outside of the cloned flanking regions in combination with antibiotic cassette-specific primers (Table S1).

Construction of complementation constructs and site directed mutagenesis

C. jejuni mutants were complemented by inserting the individual chemotaxis genes (*cheA*, *cheY*, *cheW*, *cheV*, *cheAY*, *cj0350*, *fliN*) *in trans* using the *cj0046* pseudogene, as described previously [26]. In these plasmids, the genes are expressed from the *fdxA* promoter. To make the

CheY^{D53A} substitution, pCASO59 was used as template for inverse PCR using primers CheYDA01/02 (Table S1). To make the CheY^{D7A} substitution, pCASO59 was used as template for inverse PCR using primers cheYD7AFwd/Rev (Table S1). To make the CheAΔReceiver domain construct (CheA$^{\Delta Rec}$), pCASO58 was used as template for inverse PCR using primers cheARec01/02, which changes the codon encoding lysine 648 to a stop codon (see Table S1). The inverse PCR products were digested with *Dpn*I for 60 minutes at 37°C and then purified (PCR purification kit, QIAGEN) and transformed into *E. coli*. To identify clones containing altered sequences, plasmid DNA was purified and sequenced using appropriate primers (Eurofins Genomics, Ebersberg, Germany).

RNA Extraction and RT-PCR

RNA was extracted using the hot phenol method [38]. RNA concentration was determined using a Nanodrop 2000 (Thermo Fisher Scientific). A mix of Moloney Murine Leukemia Virus (M-MuLV) Reverse Transcriptase and murine RNase Inhibitor with an optimized random primer mix was used to make cDNA (NEB). Two μg of RNA was mixed with random primers (6 μM final concentration) and water and incubated at 70°C for 5 minutes then on ice for 5 minutes. This mix was added to 10 μl of M-MuLV reaction mix and 2 μl M-MuLV enzyme mix in a total volume of 20 μl. Control reactions were also prepared containing 2 μl water in place of enzyme to show any amplification from contaminating DNA. Reactions were incubated at 25°C for 5 minutes, 42°C for 60 minutes, then 80°C for 4 minutes. Reactions were made to total volume of 50 μl by adding 30 μl water. For PCR, 2 μl of cDNA was mixed with OneTaq HotStart master mix (1× final concentration, NEB), and gene-specific primers (0.2 μM final concentration) (Table S1) in a total volume of 25 μl. Extension reactions were carried out at 68°C.

143 **Assessment of growth**

144 A 50 µl single-use glycerol stock, routinely stored at -80°C, was used to inoculate a BAB plate
145 with Skirrow supplements and these cells were used to inoculate fresh Brucella broth. Cultures were
146 grown in microaerobic conditions with shaking overnight at 37°C. The overnight culture was
147 diluted to $A_{600} \approx 0.05$ (~ 1×10^7 CFU ml^{-1}) in 200 µl in a 96-well plate (flat bottom, non-treated,
148 sterile, polystyrene, (Corning, NY, USA)). Growth in 96-well plates was assessed using an Omega
149 plate reader (FLUOstar Omega (BMG Labtech, Germany)) linked to an atmospheric control unit in
150 microaerobic conditions at 37°C. Omega assays were run for 24 hours (double orbital shaking at
151 400 rpm) and A_{600} data was recorded every 60 minutes.
152
153 **Light microscopy and flagella staining using the Ryu stain**
154 Typically, 10 µl of an overnight culture was examined using an Eclipse 50i microscope (×100
155 lens) to monitor swimming phenotypes. When necessary, a Coolpix 4500 digital camera (Nikon)
156 was used to capture video (15 frames $second^{-1}$, 320×240 pixels). Video compilations were made by
157 extracting appropriate frames using ImageJ (Rasband, W.S., ImageJ, U. S. National Institutes of
158 Health, Bethesda, Maryland, USA, http://imagej.nih.gov/ij/, 1997-2014). To plot swimming
159 behaviour, individual cells were tracked using the Manual tracking plug-in for ImageJ (Fabrice
160 Cordeli, http://rsb.info.nih.gov/ij/plugins/track/track.html) then visualized using the Chemotaxis and
161 Migration Tool (Ibidi, http://ibidi.com/software/chemotaxis_and_migration_tool/). To visualise
162 flagella, cells were stained using the Ryu stain [39] as described previously [40]. ImageJ was used
163 to add a scale bar and prepare montage images.
164
165 **Chemotaxis assays**
166 Chemotactic motility was measured using soft agar motility assays and tube taxis assays [26].
167 All soft agar motility assays were carried out using Brucella soft agar in square 10 mm^2 petri plates

(Sterilin) inoculated with wildtype and three test strains, as described previously [26]. For each plate, halo size was expressed as a percentage of the corresponding wildtype and each strain was tested for significance using a one-sample t-test (alpha = 0.05), compared to a hypothetical value of 100 (GraphPad Prism 6.01). Strain-to-strain comparisons were made using a two-tailed Mann-Whitney test.

Tube taxis assays were prepared as described previously using Brucella soft agar [26]. The tubes were incubated at 37°C in air in a waterbath (Grant). Tubes were photographed after 24, 40, 48, 64, and 72 hours and the dye front was measured from the top of the agar using the ImageJ software and expressed as a percentage of the wildtype strain. Each strain was tested for significance using a one-sample t-test (alpha = 0.05) compared to a hypothetical value of 100 (GraphPad Prism 6.01) and strain-to-strain comparisons were made using a two-tailed Mann-Whitney test.

Biofilm assays

A 50 µl single-use glycerol stock, routinely stored at -80°C, was used to inoculate a BAB plate with Skirrow supplements and these cells were used to inoculate fresh Brucella broth. Cultures were grown in microaerobic conditions with shaking overnight at 37°C. The overnight culture was diluted to $A_{600} \approx 0.05$ (~ 1 x 10^7 CFU ml^{-1}) in 22 ml sterile Brucella in a 50 ml flacon tube. A twin-frost microscope slide (sterilized in 70% ethanol) was inserted into each falcon tube. Tubes were incubated at 37°C in microaerobic conditions without shaking. After 48 hours, slides were removed from the tubes using flamed-sterilized tweezers and briefly washed in water. Slides were dried in air before staining with 1% crystal violet. Unbound crystal violet was washed off with water and slides were dried in air. Biofilms were imaged using a GenePixPro microarray scanner (Axon). The photomultiplier tube (PMT) gain of either the 635 nm or 532 nm laser was adjusted to achieve a balanced image. To assess biofilm shedding, the A_{600} of the planktonic cultures were measured;

193 statistically different results were determined using a two-tailed Mann-Whitney test (GraphPad
194 Prism 6.01).
195
196 **Bioinformatic analysis.**
197 Pfam (http://pfam.sanger.ac.uk/ and InterProScan (http://www.ebi.ac.uk/Tools/pfa/iprscan/)
198 were used to search for protein domains and architectures. All BLAST searches were conducted
199 within BioEdit. EMBOSS Water was used for pairwise protein alignments
200 (http://www.ebi.ac.uk/Tools/psa/emboss_water/). ClustalX was used for multiple sequence
201 alignment (http://www.clustal.org/clustal2/). DeepView version 4.1 was used to make the CheY
202 model (http://spdbv.vital-it.ch/).
203
204 **RESULTS**
205
206 **Inactivation and complementation of the genes involved in the core chemotaxis system**
207 To assess the roles of the *cheVAWY* genes in *C. jejuni* chemotaxis, each individual gene was
208 inactivated by a kanamycin or chloramphenical antibiotic resistance cassette in the same orientation
209 as the gene. To test for polar effects, each mutated gene was complemented by introduction of the
210 different chemotaxis genes mutant *in trans* in the *cj0046* pseudogene under control of the *fdxA*
211 promoter [26]. We also used this complementation system to introduce altered versions of the *cheY*
212 and *cheA* genes in *C. jejuni* mutants, and tested the effect of alteration of expression levels by
213 introducing a second copy of chemotaxis genes in wildtype *C. jejuni* NCTC11168 (Table 1). All the
214 mutant strains did not show significant changes in growth (Fig. S1) and expressed flagella at both
215 poles (Fig. 2). For all mutants generated here, chemotactic motility was assessed using soft agar
216 motility plates and tube taxis assays, which measures motility in both an energy and redox gradient
217 [26].

218

219 **CheV is the dominant adaptor protein in the chemotaxis signalling pathway**

220 In liquid media, motility of the *cheW* and *cheV* mutants was comparable to the wildtype, but
221 both halo formation and migration were reduced compared to the wildtype (Fig. 3, Fig. S2).
222 Chemotactic motility of the *cheW* mutant was reduced to less than 50% compared to the wildtype
223 strain at both 24 and 48 hours, respectively (Fig. 3, Fig. S2). The *cheV* mutant showed greater
224 reduction in halo formation and migration than the *cheW* mutant when compared to the wildtype
225 strain at both 24 and 48 hours (Fig. 3, Fig. S2). Complementation of the *cheW* mutant restored
226 chemotaxis phenotypes to that of the wildtype strain (Fig. 3, Fig. S2). However, complementation
227 of the *cheV* mutant did not restore chemotactic motility. The *cheV* mutant still expressed the
228 downstream *cheA* and *cheW* genes as shown by reverse transcriptase PCR (Fig. S3A), suggesting
229 the phenotype of the *cheV* mutant is not due to polar effects on the transcription of the downstream
230 *cheA* and *cheW* genes. Supplementation of the wildtype strain with a second copy of *cheV* (WT
231 +*cheV*) did not alter swimming in liquid media, but led to a significant reduction in chemotactic
232 motility (Fig. S4), suggesting that the stoichiometry of CheV and other chemotaxis proteins is of
233 importance for its function. Finally, complementation of the *cheW* mutant with the *cheV* gene did
234 not restore chemotactic motility (Fig. 3, Fig. S2).

235

236 **Increased levels of CheY affect chemotactic motility**

237 The *cheY* mutant showed a 'Catherine Wheel' swimming behaviour [41] in liquid media, where
238 a cell would appear to get trapped in a clockwise swimming loop (see Supplementary Movie 1 and
239 Fig. 4B) before resuming a darting motility as observed in the wildtype (Fig. 4A). The *cheY* mutant
240 displayed the previously described chemotaxis defect [32], with chemotactic motility reduced to
241 less than 20% of wildtype (Fig. 3, Fig. S2). Chemotactic motility was restored to wildtype levels by
242 complementation with the *cheY* gene, and even exceeded that observed in the wildtype strain (Fig.

3, Fig. S2), with the wildtype swimming behaviour also restored (Fig. 4C). A wildtype strain containing an additional copy of *cheY* (WT + *cheY*) displayed increased chemotactic motility compared to the wildtype strain (Fig. S4).

CheY requires the metal binding pocket but not the phosphorylation site for activity

An alignment of the seed sequences for a canonical Receiver Domain (Pfam, PF00072) with the *C. jejuni* CheY sequence showed that both the active site aspartic acid residue (D53) and the N-terminal 'acid-pocket' aspartic acid residues (D7, D8) were well conserved (Fig. S5A). A three-dimensional model of *C. jejuni* CheY, based on the *Thermotoga maritima* CheY structure [42] shows that the three aspartic acid residues are predicted to cluster to form the active site (Fig. S5 inset). These predictions were tested experimentally using site-directed mutagenesis of aspartate residues 7 and 53 to alanine (D7A and D53A) of the *cheY* gene, to eliminate either phosphorylation or metal binding, respectively, and the mutated versions were introduced in the *cheY* mutant. The *cheY* mutant containing $cheY^{D53A}$ produced flagella (Fig. 2), and showed full restoration of wildtype phenotype with swimming without the 'Catherine Wheel' phenotype (Fig. 4D), and restoration of chemotactic motility to wildtype levels (Fig. 3, Fig. S2). In contrast, the *cheY* mutant containing $cheY^{D7A}$ was even more defective in chemotactic motility (Fig. 3, Fig. S2), despite possessing flagella (Fig. 2). The $cheY^{D7A}$ strain displayed swimming in very tight repeating spirals (Fig. 4E). RT-PCR showed that all *cheY*-complemented strains made a *cheY* transcript that was absent in the *cheY* mutant (Fig. S3D).

CheA is required for chemotaxis but the C-terminal receiver domain is not

Inactivation of the *cheA* gene strongly reduced chemotactic motility to levels similar to the *cheV* and *cheY* mutants (Fig. 3, Fig. S2). However, inactivation of *cheA* did not disrupt transcription of the downstream *cheW* gene, as determined with RT-PCR (Fig. S3B) Introduction of the *cheA*

gene *in trans* did not complement the *cheA* mutant (Fig. 3, Fig. S2), but introduction of a second *cheA* copy in the wildtype strain resulted in significantly reduced chemotactic motility (Fig. S4).

The architecture of *C. jejuni* CheA differs to that seen in *E. coli* and *B. subtilis* (Fig. 1), as it has a C-terminal receiver domain, CheA-Y, with 58% similarity (33% identity) to CheY (Fig. S5B). The multiple alignment of CheY sequences including CheA-Y shows the presence of two aspartic acid residues at the N-terminus and the active site aspartate, suggesting that the acid-pocket active site is conserved (Fig. S5A). To assess the role of the CheA-Y domain in the function of CheA, the *cheA* gene was mutated to contain a stop-codon at position 648 ($cheA^{\Delta Rec}$), truncating the CheA protein at the start of the C-terminal receiver domain. Introduction of the $cheA^{\Delta Rec}$ gene in the wildtype and *cheA* mutant strain resulted in transcription of a *cheA* transcript, which was absent in the *cheA* mutant (Fig. S3E). The $cheA^{\Delta Rec}$ construct complemented the *cheA* mutant better than the full length *cheA* gene, with restoration of about half of chemotactic motility by the $cheA^{\Delta Rec}$ version, and no complementation by the wildtype *cheA* gene (Fig. 3, Fig. S2). When the $cheA^{\Delta Rec}$ gene was introduced into the wildtype strain, this resulted in increased levels of chemotactic motility compared to the wildtype strain (Fig. S4). We also investigated the ability of the CheA-Y receiver domain alone to complement the *cheY* mutant, but this did not restore chemotactic motility (Fig. 3, Fig. S2, Fig. S3), and the swimming behaviour still showed the characteristic catherine wheels seen in the *cheY* mutant (Fig. 4). Thus, the sequence of the CheA-Y domain has diverged to the point where it is functionally distinct from CheY in *C. jejuni*.

The *C. jejuni cj0350* gene encodes a putative CheX protein

A domain search of the NCTC11168 genome identified the *cj0350* gene as encoding a putative CheX domain. CheX is an ancillary chemotaxis protein known to dephosphorylate CheY in *Borrelia burgdorferi* [43] and *Thermotoga maritima* [44]. The *C. jejuni* CheX sequence is well conserved in the genus *Campylobacter* (but absent from the genus *Helicobacter*), although

293 divergent from the canonical CheX sequences that comprise the Pfam seed alignment PF13690. We
294 constructed a *cj0350* mutant, which showed decreased chemotactic motility, although this
295 phenotype was not rescued by complementation with *cj0350* (Fig. 5). However, complementation
296 by the gene downstream of *cj0350*, *fliN*, did restore wildtype chemotactic motility (Fig. 5),
297 suggesting that the *cj0350* (*cheX*) phenotype is probably due to a disruption of *fliN* expression.
298 Introduction of a second copy of the *cj0350* gene in wildtype *C. jejuni* did not affect flagellar
299 assembly (Fig. 5D) or swimming in liquid media (see Supplementary Movie 2), but resulted in
300 reduced chemotactic motility (Fig. 5A-C). Given that phosphatase activity on CheY should result in
301 decreased chemotactic motility due to less stimulation of the flagella switch, this is consistent with
302 the possibility that Cj0350 is a divergent CheX ortholog.
303
304 **Chemotaxis is required for organized biofilm formation at the air-media interface**
305 We investigated the role of chemotaxis in biofilm formation, by developing a glass-slidebased
306 assay combined with crystal violet staining, with detection using a microarray scanner (employing
307 both lasers at 532 and 635 nm). The wildtype strain formed a biofilm on the glass slide at the air-
308 media interface (Fig. 6). Below the air-media interface, a less-intense ~2 mm band of adhered cells
309 was observed. All of the chemotaxis mutants used in this study were defective in formation of a
310 biofilm at the air-media interface (Fig. 6). In the *cheW* mutant, the air-media interface biofilm was
311 present, but a second more intense area of adhered cells was also visible ~5 mm below the air-
312 media interface. Both the *cheV* mutant and the complemented *cheV* mutant showed defective air-
313 media interface biofilm. The *cheA* and *cheY* mutants both showed a disorganized air-media
314 interface biofilm with a greater population of submerged cells. In all cases, except for the *cheV*
315 mutant and the $cheY^{D7A}$-complemented *cheY* mutant, complementation with the respective wildtype
316 gene restored the organised interface biofilm phenotype (Fig. 6). To assess the level of shedding of
317 cells from the biofilm, the A_{600} of planktonic fraction for each assay was recorded. Inactivation of

318 *cheY* resulted in fewer cells in the planktonic fraction compared to the wildtype strain, while the
319 complemented *cheY* mutant and the *cheY*^{D53A} complemented mutant both had more cells in the
320 planktonic fraction (Fig. S6A). Other *cheY* strains with reduced chemotactic motility also showed a
321 lower level of cells in the planktonic fraction. Therefore, the biofilm phenotype of at least the *cheY*
322 mutant could in part be due to a disruption of normal cell shedding/dispersal from the biofilm. To
323 test the hypothesis that *C. jejuni* may require the fully functional chemotactic motility to seek the
324 optimal environment for growth as a biofilm, the slide biofilm assay was performed using a
325 paralysed flagella (*pflA*) mutant [40, 45]. This mutant displayed low levels of biofilm formation at
326 the air-media interface (Fig. S6B). Thus, while the chemotaxis system is not required for biofilm
327 formation *per se*, it is necessary for organized biofilm formation at the air-media interface and may
328 play a role in dispersal/shedding of cells from the biofilm.
329
330 **DISCUSSION**
331 Flagellar motility plays an important role in colonisation and virulence of many bacterial
332 pathogens. While the ability to move to or from locations is an important contributor to the
333 infection process, such movement needs to be directed, and is commonly based on detection of
334 external (e.g. chemical gradient) and internal stimuli (e.g. metabolic state). These stimuli can be
335 positive or negative, with examples of positive stimuli being attractants such as nutrients, while
336 negative stimuli can be repellents such as bile acids. The chemotaxis system integrates the signals
337 from external and internal sensors through a signal transduction cascade consisting of MCPs,
338 CheW/CheV, CheA and CheY, while other factors such as CheB, CheR, CheC, CheZ, or CheX may
339 modulate and fine-tune the signal transduction cascade, with diverse combinations observed
340 throughout the bacterial kingdom [4, 46].
341 In this study we have dissected the core chemotaxis signalling pathway of the important
342 foodborne zoonotic pathogen *C. jejuni*, which is the most common bacterial cause of gastroenteritis

in the developed world. Directed motility is central to the process of intestinal colonisation by *C. jejuni*, as mutants defective in motility or chemotaxis are either unable to colonise or show significantly reduced efficiency of colonisation [32, 36]. Although *C. jejuni* shares many components of the core chemotaxis pathway with model organisms such as *E. coli* and *B. subtilis*, its chemotaxis system contains several additional components and modifications, and in this study we have used a combination of gene inactivation and complementation experiments with phenotypic assays to study the *C. jejuni* chemotaxis system.

Roles of *C. jejuni* CheW and CheV adaptor proteins in chemotaxis

Campylobacter is not exceptional in containing both CheV and CheW proteins. Although CheW is the most common chemotaxis 'adaptor' protein (found in nearly 100% of genomes containing the core chemotaxis components [47], CheV was found in almost 40% of chemotaxis-positive genomes [47] and three genomes (*B. thuringiensis*, *B. weihenstephanensis*, and *L. monocytogenes*) were found to contain CheV orthologs without CheW orthologs, suggesting that CheV alone can function in the MCP-CheA complex [47]. In this study, the chemotaxis phenotype of the *cheW* mutant is the least severe, suggesting that CheV does function to elicit some signal transduction event. Similar effects were observed in *B. subtilis* [48] and further showed that the CheW domain of CheV was sufficient for signal transduction. A direct protein-protein interaction between CheV and Tlp4 (deoxycholate sensor, Cj0262c), Tlp6 (TCA intermediates sensor, Cj0448c), and Tlp8 (redox sensor CetZ) has been documented [49] and Yeast Two- and Three-Hybrid analysis and immunoprecipitation were used to show that Tlp1 interacts with both CheW and CheV, although the interaction with CheV was much stronger and localised to the CheV-W domain [50]. Both *cheV* and *cheW* mutants had chemotactic motility defects in Brucella media although chemotaxis towards aspartate was still competent in either mutant. Similarly, the novel chemotaxis protein Cj0371 of *C. jejuni* was shown to interact with the CheV protein, and influence

ATPase activity of CheA [51], suggesting that multiple systems engage in the chemotaxis pathway to modulate signal transduction. An evolutionary genomics study showed that the presence of CheV is correlated with increased numbers of MCPs and proposed that CheV functions to accommodate signal transduction from a specific group of MCPs, exemplified by the *Salmonella* McpC chemoreceptor [19]. None of the ten *C. jejuni* MCPs share the architecture of the McpC-type sensor. Moreover, *H. pylori* genomes encode only four chemotaxis sensors and three CheV proteins [52]. The C-terminal receiver domain on CheV most likely refines the function of this protein. It has previously been proposed that CheV acts as a phosphate sink, normalizing over-stimulation of CheA [19, 53, 54]. The observation that expressing two copies of CheV in *C. jejuni* reduces chemotactic motility (Fig. 3, Fig. S2) supports this theory, as increasing the level of the CheV protein will divert phosphate flow from CheY to CheV. Interestingly, the chemotaxis phenotype of the WT +*cheV* strain was more pronounced than that of the WT +*cheX* strain, which suggests that the phosphate sink is more effective at dampening signal transduction than the possible CheX-mediated dephosphorylation of CheY. Organisms lacking CheY-phosphatases may also utilize a phosphate sink mechanism to modulate chemotaxis.

Role of CheY domains

The CheY protein is the final effector protein in the signal transduction cascade, directly interacting with the flagellar switch to alter rotation between clockwise and counter-clockwise rotation. Our observation that the *cheY*^{D53A} variant could restore both chemotactic motility and darting swimming in the *cheY* mutant (Fig. 3, Fig. S2) suggests that either a) unphosphorylated CheY can interact with the flagella switch or b) the conserved aspartate 53 residue is not the only site of activating phosphorylation. Sequence alignment of *C. jejuni* CheY with the seed receiver domain alignment unambiguously identifies the putative site of phosphorylation and a structural model clearly places Aspartate 53 in the acid pocket active site. Expression of CheY^{D53A} from the

393 *fdxA* promoter may result in expression of the protein at increased levels. Indeed, expression of
394 wildtype CheY from the *fdxA* promoter significantly stimulated chemotactic motility (Fig. 3, Fig.
395 S2). Based on the CheY^{D53A} data, the chemotactic motility observed in the complemented *cheY*
396 mutant may be a mixture of CheY and CheY-P interaction at the flagella switch. If
397 unphosphorylated CheY can modify the flagella switch operation, the question of resetting the
398 chemotaxis system in *C. jejuni* becomes all the more intriguing. If one further considers the C-
399 terminal receiver domain of CheA as a further phosphate sink, the complete model of phosphate-
400 flow in *C. jejuni* chemotaxis becomes a complex story. The CheA-Y domain has all the hallmarks
401 of the classical receiver domain and appears to be dispensable for the core signal transduction
402 function. Moreover, CheA-Y is no substitute for CheY as the *cheA-Y* gene could not complement
403 the inactivation of *cheY* (Fig. 3, Fig. S2). Residues that are known to be important for binding the
404 flagella switch (T87, Y106, and K109 (*E. coli* numbering [55])) are conserved in CheA-Y and
405 amino acid differences between CheY and CheA-Y are spread across the entire sequence, and not
406 localized to the β4-α4 region, which shows the largest structural changes following phosphorylation
407 [56, 57]. Sequence divergence resulting in loss of chemotactic function is well documented: *R.*
408 *sphaeroides che* genes only partially restore taxis in *E. coli* [58]. Thus, the *C. jejuni* CheY/CheA-Y
409 proteins provide a good model for studying mutational drift resulting in loss or change of function.
410 *C. jejuni* CheA lacks the P2 domain found in *E. coli* and *B. subtilis* CheA (Fig. 1), which raises the
411 question of how it interacts with CheY. In *C jejuni*, CheA and CheY interact with each other [49].
412 However, since CheA$^{\Delta Rec}$ restores signalling, the CheA-Y domain is not the likely interaction
413 partner for CheY.
414
415 **Other components of the chemotaxis pathway**
416 In this study we have identified the *cj0350* gene as a potential new chemotaxis gene in *C.*
417 *jejuni*. Although inactivation of the *cj0350* gene did affect chemotaxis, this could be explained by a

polar effect on the downstream *fliN* flagellar gene, and hence we cannot be certain about the role of Cj0350 in chemotaxis yet. Motif analysis suggests the Cj0350 protein may be a novel variant of the CheX phosphatase, representing a *Campylobacter*-specific chemotaxis adaptation in the Epsilonproteobacteria, as no CheX ortholog could be detected in any available *Helicobacter* genome. The primary sequence of the putative CheX protein identified in this study is divergent from the canonical CheX sequence. Thus, in organisms where no current phosphatase has been identified, cryptic phosphatase proteins may yet be discovered. In addition to CheX and CheZ, a number of other CheY phosphatases have been characterized. *B. subtilis* uses CheC, CheD, and a FliY/N fusion protein [59-61]. However, chemotaxis systems lacking any clear phosphatases are also known (~20% of chemotaxis positive genomes [47]); for instance, *R. sphaeroides*, *Rhodospirillum centenum*, and *Sinorhizobium meliloti* have complex chemotaxis systems but lack known CheY-phosphatases [22, 58]. *H. pylori* further regulates CheZ activity by complex formation with the novel chemotaxis protein ChePep [20, 62]. *Campylobacter jejuni* contains a ChePep homolog (NCTC11168 - Cj1178c), which can complement an *H. pylori chepep* mutant [62] although the role of this protein in chemotaxis in *C. jejuni* is currently not known.

Chemotaxis and biofilm formation

Previous studies have implicated chemotaxis sensors in biofilm formation. Tlp3 (Cj1564) mutants showed increased biofilm formation [63], while CetZ (Tlp8) mutants showed decreased biofilm formation [33]. We show that removing each component of the chemotaxis pathway results in disruption of biofilm formation at a discrete air-surface interface, and that this phenotype can be rescued by complementation for most of the chemotaxis genes investigated here. Thus, the chemotaxis system likely has a role in coordinating biofilm formation, and this coordinating role may extend to shedding and dispersal of cells from the biofilm. This study is therefore the first to present a role for signal transduction in the active dispersal of cells from a *C. jejuni* biofilm. In

443 processing environments, biofilms present a reservoir of cells that can subsequently re-contaminate
444 the food chain highlighting the need to learn more about biofilm dispersal.
445
446 **Conclusions**
447 The ability to couple flagella rotation with environmental sensing is an effective adaptive
448 mechanism allowing bacteria to seek an optimum environment. While chemotaxis systems from
449 model organisms such as *E. coli* and *B. subtilis* provide an effective model for studying signal
450 transduction in non-paradigm organisms, species-specific modulations and augmentations abound
451 and require focussed investigation. Such genus- and species-specific analyses will be required to
452 better understand chemotaxis in other Epsilon-proteobacteria and other organisms that share
453 elements of the *Campylobacter* chemotaxis system and provides a further paradigm for chemotaxis
454 signal transduction.
455
456 **ACKNOWLEDGMENTS**
457 The authors wish to thank Dr Henri Tapp for assistance with statistical evaluations, and members of
458 the former IFR *Campylobacter* research group for helpful discussions. We would also like to thank
459 Rachael Stanley for electron microscopy and Maddy Houchen and Robert Hindmarsh for
460 microbiology media support.
461
462 **FUNDING STATEMENT**
463 The authors gratefully acknowledge the support of the Biotechnology and Biological Sciences
464 Research Council (BBSRC) via the Gut Health and Food Safety Institute Strategic Programme
465 (BB/J004529/1). The funder had no role in study design, data collection and analysis, decision to
466 publish, or preparation of the manuscript.
467

CONFLICTS OF INTEREST

The authors declare that there are no conflicts of interest.

REFERENCES

1. **Nichols GL, Richardson JF, Sheppard SK, Lane C, Sarran C**. Campylobacter epidemiology: a descriptive study reviewing 1 million cases in England and Wales between 1989 and 2011. *BMJ Open* 2012;2:e001179. doi: 10.1136/bmjopen-2012-001179
2. **Tam CC, Higgins CD, Neal KR, Rodrigues LC, Millership SE et al.** Chicken Consumption and Use of Acid-Suppressing Medications as Risk Factors for Campylobacter Enteritis, England. *Emerg Infect Dis* 2009;15:1402-1408. doi: 10.3201/eid1509.080773
3. **Poropatich KO, Walker CL, Black RE**. Quantifying the association between Campylobacter infection and Guillain-Barre syndrome: a systematic review. *J Health Popul Nutr* 2010;28:545-52. doi:
4. **Lertsethtakarn P, Ottemann KM, Hendrixson DR**. Motility and chemotaxis in Campylobacter and Helicobacter. *Annu Rev Microbiol* 2011;65:389-410. doi: 10.1146/annurev-micro-090110-102908
5. **Gao B, Lara-Tejero M, Lefebre M, Goodman AL, Galan JE**. Novel components of the flagellar system in epsilonproteobacteria. *MBio* 2014;5:e01349-14. doi: 10.1128/mBio.01349-14
6. **Asakura H, Hashii N, Uema M, Kawasaki N, Sugita-Konishi Y et al.** Campylobacter jejuni pdxA affects flagellum-mediated motility to alter host colonization. *PLoS One* 2013;8:e70418. doi: 10.1371/journal.pone.0070418
7. **Reuter M, Mallett A, Pearson BM, van Vliet AHM**. Biofilm formation by *Campylobacter jejuni* is increased under aerobic conditions. *Appl Environ Microbiol* 2010;76:2122-8. doi: 10.1128/AEM.01878-09
8. **Svensson SL, Pryjma M, Gaynor EC**. Flagella-mediated adhesion and extracellular DNA release contribute to biofilm formation and stress tolerance of Campylobacter jejuni. *PLoS One* 2014;9:e106063. doi: 10.1371/journal.pone.0106063
9. **Brown HL, Reuter M, Salt LJ, Cross KL, Betts RP et al.** Chicken juice enhances surface attachment and biofilm formation of Campylobacter jejuni. *Appl Environ Microbiol* 2014;80:7053-60. doi: 10.1128/AEM.02614-14
10. **Baldvinsson SB, Sorensen MC, Vegge CS, Clokie MR, Brondsted L**. Campylobacter jejuni motility is required for infection of the flagellotropic bacteriophage F341. *Appl Environ Microbiol* 2014;80:7096-106. doi: 10.1128/AEM.02057-14
11. **Korolik V**. The role of chemotaxis during Campylobacter jejuni colonisation and pathogenesis. *Curr Opin Microbiol* 2018;47:32-37. doi: 10.1016/j.mib.2018.11.001
12. **Hazelbauer GL, Lai WC**. Bacterial chemoreceptors: providing enhanced features to two-component signaling. *Curr Opin Microbiol* 2010;13:124-32. doi: 10.1016/j.mib.2009.12.014
13. **Patteson AE, Gopinath A, Goulian M, Arratia PE**. Running and tumbling with E. coli in polymeric solutions. *Sci Rep* 2015;5:15761. doi: 10.1038/srep15761
14. **Krell T, Lacal J, Munoz-Martinez F, Reyes-Darias JA, Cadirci BH et al.** Diversity at its best: bacterial taxis. *Environ Microbiol* 2011;13:1115-24. doi: 10.1111/j.1462-2920.2010.02383.x
15. **Cluzel P, Surette M, Leibler S**. An ultrasensitive bacterial motor revealed by monitoring signaling proteins in single cells. *Science* 2000;287:1652-5. doi:
16. **Martin AC, Wadhams GH, Armitage JP**. The roles of the multiple CheW and CheA homologues in chemotaxis and in chemoreceptor localization in *Rhodobacter sphaeroides*. *Mol Microbiol* 2001;40:1261-72. doi:
17. **Boukhvalova MS, Dahlquist FW, Stewart RC**. CheW binding interactions with CheA and Tar. Importance for chemotaxis signaling in *Escherichia coli*. *J Biol Chem* 2002;277:22251-9. doi: 10.1074/jbc.M110908200

18. **Parkinson JS, Hazelbauer GL, Falke JJ**. Signaling and sensory adaptation in *Escherichia coli* chemoreceptors: 2015 update. *Trends Microbiol* 2015;23:257-266. doi: 10.1016/j.tim.2015.03.003
19. **Ortega DR, Zhulin IB**. Evolutionary Genomics Suggests That CheV Is an Additional Adaptor for Accommodating Specific Chemoreceptors within the Chemotaxis Signaling Complex. *PLoS computational biology* 2016;12:e1004723. doi: 10.1371/journal.pcbi.1004723
20. **Lertsethtakarn P, Howitt MR, Castellon J, Amieva MR, Ottemann KM**. *Helicobacter pylori* CheZ(HP) and ChePep form a novel chemotaxis-regulatory complex distinct from the core chemotaxis signaling proteins and the flagellar motor. *Mol Microbiol* 2015;97:1063-78. doi: 10.1111/mmi.13086
21. **Muff TJ, Foster RM, Liu PJ, Ordal GW**. CheX in the three-phosphatase system of bacterial chemotaxis. *J Bacteriol* 2007;189:7007-13. doi: 10.1128/JB.00896-07
22. **Porter SL, Wadhams GH, Armitage JP**. Signal processing in complex chemotaxis pathways. *Nat Rev Microbiol* 2011;9:153-65. doi: 10.1038/nrmicro2505
23. **Day CJ, King RM, Shewell LK, Tram G, Najnin T et al.** A direct-sensing galactose chemoreceptor recently evolved in invasive strains of Campylobacter jejuni. *Nat Commun* 2016;7:13206. doi: 10.1038/ncomms13206
24. **Li Z, Lou H, Ojcius DM, Sun A, Sun D et al.** Methyl-accepting chemotaxis proteins 3 and 4 are responsible for *Campylobacter jejuni* chemotaxis and jejuna colonization in mice in response to sodium deoxycholate. *J Med Microbiol* 2014;63:343-54. doi: 10.1099/jmm.0.068023-0
25. **Vegge CS, Brondsted L, Li YP, Bang DD, Ingmer H**. Energy taxis drives *Campylobacter jejuni* toward the most favorable conditions for growth. *Appl Environ Microbiol* 2009;75:5308-14. doi: 10.1128/aem.00287-09
26. **Reuter M, van Vliet AHM**. Signal balancing by the CetABC and CetZ chemoreceptors controls energy taxis in *Campylobacter jejuni*. *PLoS One* 2013;8:e54390. doi: 10.1371/journal.pone.0054390
27. **Dwivedi R, Nothaft H, Garber J, Xin Kin L, Stahl M et al.** L-fucose influences chemotaxis and biofilm formation in *Campylobacter jejuni*. *Mol Microbiol* 2016;101:575-589. doi: 10.1111/mmi.13409
28. **Lubke AL, Minatelli S, Riedel T, Lugert R, Schober I et al.** The transducer-like protein Tlp12 of Campylobacter jejuni is involved in glutamate and pyruvate chemotaxis. *BMC Microbiol* 2018;18:111. doi: 10.1186/s12866-018-1254-0
29. **Chandrashekhar K, Srivastava V, Hwang S, Jeon B, Ryu S et al.** Transducer-Like Protein in Campylobacter jejuni With a Role in Mediating Chemotaxis to Iron and Phosphate. *Front Microbiol* 2018;9:2674. doi: 10.3389/fmicb.2018.02674
30. **Cha G, Chen Z, Mo R, Lu G, Gao B**. The Novel Regulators CheP and CheQ Control the Core Chemotaxis Operon cheVAW in Campylobacter jejuni. *Mol Microbiol* 2018:Epub ahead of print, doi: 10.1111/mmi.14144. doi: 10.1111/mmi.14144
31. **Takata T, Fujimoto S, Amako K**. Isolation of nonchemotactic mutants of *Campylobacter jejuni* and their colonization of the mouse intestinal tract. *Infect Immun* 1992;60:3596-600. doi:
32. **Yao R, Burr DH, Guerry P**. CheY-mediated modulation of *Campylobacter jejuni* virulence. *Mol Microbiol* 1997;23:1021-31. doi:
33. **Chandrashekhar K, Gangaiah D, Pina-Mimbela R, Kassem, II, Jeon BH et al.** Transducer like proteins of *Campylobacter jejuni* 81-176: role in chemotaxis and colonization of the chicken gastrointestinal tract. *Front Cell Infect Microbiol* 2015;5:46. doi: 10.3389/fcimb.2015.00046
34. **Hendrixson DR, DiRita VJ**. Identification of *Campylobacter jejuni* genes involved in commensal colonization of the chick gastrointestinal tract. *Mol Microbiol* 2004;52:471-84. doi: 10.1111/j.1365-2958.2004.03988.x

35. **Bereswill S, Fischer A, Plickert R, Haag LM, Otto B et al.** Novel murine infection models provide deep insights into the "menage a trois" of *Campylobacter jejuni*, microbiota and host innate immunity. *PLoS One* 2011;6:e20953. doi: 10.1371/journal.pone.0020953
36. **de Vries SP, Linn A, Macleod K, MacCallum A, Hardy SP et al.** Analysis of Campylobacter jejuni infection in the gnotobiotic piglet and genome-wide identification of bacterial factors required for infection. *Sci Rep* 2017;7:44283. doi: 10.1038/srep44283
37. **Gao B, Vorwerk H, Huber C, Lara-Tejero M, Mohr J et al.** Metabolic and fitness determinants for in vitro growth and intestinal colonization of the bacterial pathogen Campylobacter jejuni. *PLoS Biol* 2017;15:e2001390. doi: 10.1371/journal.pbio.2001390
38. **Porcelli I, Reuter M, Pearson BM, Wilhelm T, van Vliet AHM**. Parallel evolution of genome structure and transcriptional landscape in the Epsilonproteobacteria. *BMC Genomics* 2013;14:616. doi: 10.1186/1471-2164-14-616
39. **Heimbrook ME, Wang WL, Campbell G**. Staining bacterial flagella easily. *J Clin Microbiol* 1989;27:2612-5. doi:
40. **Reuter M, Periago PM, Mulholland F, Brown HL, van Vliet AHM**. A PAS domain-containing regulator controls flagella-flagella interactions in *Campylobacter jejuni*. *Front Microbiol* 2015;6:770. doi: 10.3389/fmicb.2015.00770
41. **Lauga E, DiLuzio WR, Whitesides GM, Stone HA**. Swimming in circles: motion of bacteria near solid boundaries. *Biophys J* 2006;90:400-12. doi: 10.1529/biophysj.105.069401
42. **Usher KC, de la Cruz AF, Dahlquist FW, Swanson RV, Simon MI et al.** Crystal structures of CheY from Thermotoga maritima do not support conventional explanations for the structural basis of enhanced thermostability. *Protein Sci* 1998;7:403-12. doi: 10.1002/pro.5560070221
43. **Motaleb MA, Miller MR, Li C, Bakker RG, Goldstein SF et al.** CheX is a phosphorylated CheY phosphatase essential for *Borrelia burgdorferi* chemotaxis. *J Bacteriol* 2005;187:7963-9. doi: 10.1128/jb.187.23.7963-7969.2005
44. **Park SY, Chao X, Gonzalez-Bonet G, Beel BD, Bilwes AM et al.** Structure and function of an unusual family of protein phosphatases: the bacterial chemotaxis proteins CheC and CheX. *Mol Cell* 2004;16:563-74. doi: 10.1016/j.molcel.2004.10.018
45. **Yao R, Burr DH, Doig P, Trust TJ, Niu H et al.** Isolation of motile and non-motile insertional mutants of *Campylobacter jejuni*: the role of motility in adherence and invasion of eukaryotic cells. *Mol Microbiol* 1994;14:883-93. doi:
46. **Micali G, Endres RG**. Bacterial chemotaxis: information processing, thermodynamics, and behavior. *Curr Opin Microbiol* 2016;30:8-15. doi: 10.1016/j.mib.2015.12.001
47. **Wuichet K, Zhulin IB**. Origins and Diversification of a Complex Signal Transduction System in Prokaryotes. *Science Signaling* 2010;3:ra50-ra50. doi: 10.1126/scisignal.2000724
48. **Rosario MM, Fredrick KL, Ordal GW, Helmann JD**. Chemotaxis in Bacillus subtilis requires either of two functionally redundant CheW homologs. *J Bacteriol* 1994;176:2736-9. doi:
49. **Parrish JR, Yu J, Liu G, Hines JA, Chan JE et al.** A proteome-wide protein interaction map for *Campylobacter jejuni*. *Genome Biol* 2007;8:R130. doi: 10.1186/gb-2007-8-7-r130
50. **Hartley-Tassell LE, Shewell LK, Day CJ, Wilson JC, Sandhu R et al.** Identification and characterization of the aspartate chemosensory receptor of *Campylobacter jejuni*. *Mol Microbiol* 2010;75:710-30. doi: 10.1111/j.1365-2958.2009.07010.x
51. **Du X, Wang N, Ren F, Tang H, Jiao X et al.** cj0371: A Novel Virulence-Associated Gene of Campylobacter jejuni. *Front Microbiol* 2016;7:1094. doi: 10.3389/fmicb.2016.01094
52. **Jimenez-Pearson MA, Delany I, Scarlato V, Beier D**. Phosphate flow in the chemotactic response system of *Helicobacter pylori*. *Microbiology (Reading, England)* 2005;151:3299-311. doi: 10.1099/mic.0.28217-0

53. **Karatan E, Saulmon MM, Bunn MW, Ordal GW**. Phosphorylation of the response regulator CheV is required for adaptation to attractants during *Bacillus subtilis* chemotaxis. *J Biol Chem* 2001;276:43618-26. doi: 10.1074/jbc.M104955200
54. **Pittman MS, Goodwin M, Kelly DJ**. Chemotaxis in the human gastric pathogen *Helicobacter pylori*: different roles for CheW and the three CheV paralogues, and evidence for CheV2 phosphorylation. *Microbiology (Reading, England)* 2001;147:2493-504. doi: 10.1099/00221287-147-9-2493
55. **Schuster M, Silversmith RE, Bourret RB**. Conformational coupling in the chemotaxis response regulator CheY. *Proc Natl Acad Sci U S A* 2001;98:6003-8. doi: 10.1073/pnas.101571298
56. **Sola M, Lopez-Hernandez E, Cronet P, Lacroix E, Serrano L et al.** Towards understanding a molecular switch mechanism: thermodynamic and crystallographic studies of the signal transduction protein CheY. *J Mol Biol* 2000;303:213-25. doi: 10.1006/jmbi.2000.4507
57. **Lee SY, Cho HS, Pelton JG, Yan D, Berry EA et al.** Crystal structure of activated CheY. Comparison with other activated receiver domains. *J Biol Chem* 2001;276:16425-31. doi: 10.1074/jbc.M101002200
58. **Porter SL, Wadhams GH, Armitage JP**. *Rhodobacter sphaeroides*: complexity in chemotactic signalling. *Trends Microbiol* 2008;16:251-60. doi: 10.1016/j.tim.2008.02.006
59. **Szurmant H, Bunn MW, Cannistraro VJ, Ordal GW**. Bacillus subtilis hydrolyzes CheY-P at the location of its action, the flagellar switch. *J Biol Chem* 2003;278:48611-6. doi: 10.1074/jbc.M306180200
60. **Szurmant H, Muff TJ, Ordal GW**. Bacillus subtilis CheC and FliY are members of a novel class of CheY-P-hydrolyzing proteins in the chemotactic signal transduction cascade. *J Biol Chem* 2004;279:21787-92. doi: 10.1074/jbc.M311497200
61. **Silversmith RE**. Auxiliary phosphatases in two-component signal transduction. *Curr Opin Microbiol* 2010;13:177-83. doi: 10.1016/j.mib.2010.01.004
62. **Howitt MR, Lee JY, Lertsethtakarn P, Vogelmann R, Joubert LM et al.** ChePep controls *Helicobacter pylori* Infection of the gastric glands and chemotaxis in the Epsilonproteobacteria. *MBio* 2011;2. doi: 10.1128/mBio.00098-11
63. **Rahman H, King RM, Shewell LK, Semchenko EA, Hartley-Tassell LE et al.** Characterisation of a multi-ligand binding chemoreceptor CcmL (Tlp3) of *Campylobacter jejuni*. *PLoS Pathog* 2014;10:e1003822. doi: 10.1371/journal.ppat.1003822
64. **Parkhill J, Wren BW, Mungall K, Ketley JM, Churcher C et al.** The genome sequence of the food-borne pathogen *Campylobacter jejuni* reveals hypervariable sequences. *Nature* 2000;403:665-8. doi: 10.1038/35001088

654 **Table 1.** *Campylobacter jejuni* strains used in this study.

Strain	Description [a]
***C. jejuni* strains**	
NCTC 11168	Wildtype *C. jejuni* [64]
11168 Δ*cheY*	NCTC 11168 *cj1118c::kan*^{R}
11168 Δ*cheW*	NCTC 11168 *cj0283c::kan*^{R}
11168 Δ*cheA*	NCTC 11168 *cj0284c::cat*^{R}
11168 Δ*cheV*	NCTC 11168 *cj0285c::kan*^{R}
11168 Δ*cheY* +*cheY*^{fdxApr*}	NCTC 11168 *cj1118c::kan*^{R} *cj0046*::*cj1118c*^{fdxApr}∗*cat*^{R}
11168 Δ*cheY* +*cheYD53A*^{fdxApr*}	NCTC 11168 *cj1118c::kan*^{R} *cj0046*::*cj1118c*^{D53AfdxApr}∗*cat*^{R}
11168 Δ*cheY* +*cheYD7A*^{fdxApr*}	NCTC 11168 *cj1118c::kan*^{R} *cj0046*::*cj1118c*^{D7AfdxApr}∗*cat*^{R}
11168 Δ*cheY* +*cheA-Y*^{fdxApr*}	NCTC 11168 *cj1118c::kan*^{R} *cj0046*::*cj0284c*$^{648\text{-}769\_fdxApr}$∗*cat*^{R}
11168 Δ*cheW* +*cheW*^{fdxApr*}	NCTC 11168 *cj0283c::kan*^{R} *cj0046*::*cj0283c*^{fdxApr}∗*cat*^{R}
11168 Δ*cheA* +*cheA*^{fdxApr*}	NCTC 11168 *cj0284c::cat*^{R} *cj0046*::*cj0284c*^{fdxApr}∗*kan*^{R}
11168 Δ*cheA* +*cheARec*^{fdxApr*}	NCTC 11168 *cj0284c::cat*^{R} *cj0046*::*cj0284c*ΔRec^{fdxApr}∗*kan*^{R}
11168 Δ*cheV* +*cheV*^{fdxApr*}	NCTC 11168 *cj0285c::kan*^{R} *cj0046*::*cj0285c*^{fdxApr}∗*cat*^{R}
11168 Δ*cheW* +*cheV*^{fdxApr*}	NCTC 11168 *cj0283c::kan*^{R} *cj0046*::*cj0285c*^{fdxApr}∗*cat*^{R}
11168 *cheY*^{fdxApr*}	NCTC 11168 *cj0046*::*cj1118c*^{fdxApr}∗*cat*^{R}
11168 *cheYD53A*^{fdxApr*}	NCTC 11168 *cj0046*::*cj1118c*^{D53AfdxApr}∗*cat*^{R}
11168 *cheW*^{fdxApr*}	NCTC 11168 *cj0046*::*cj0283c*^{fdxApr}∗*cat*^{R}
11168 *cheA*^{fdxApr*}	NCTC 11168 *cj0046*::*cj0284c*^{fdxApr}∗*kan*^{R}
11168 Δ*cj0350*	NCTC 11168 *cj0350::cat*^{R}
11168 *cj0350*^{fdxApr*}	NCTC 11168 *cj0046*::*cj0350*^{fdxApr}∗*kan*^{R}
11168 Δ*cj0350* +*cj0350*^{fdxApr*}	NCTC 11168 *cj0350::cat*^{R} *cj0046*::*cj0350*^{fdxApr}∗*kan*^{R}
11168 Δ*cj0350* +*fliN*^{fdxApr*}	NCTC 11168 *cj0350::cat*^{R} *cj0046*::*cj0351*^{fdxApr}∗*kan*^{R}
11168 Δ*pflA*	NCTC11168 *cj1565c::kan*^{R}

655 a. *kan*^{R}, kanamycin resistance cassette; *cat*^{R}, chloramphenicol resistance cassette; * denotes
656 complementation construct: ^{fdxApr}, gene under control of the constitutive *fdxA* promoter.

657

LEGENDS TO FIGURES

Figure 1. Architecture of the core CheV-A-W-Y chemotaxis system in *C. jejuni* compared to a model Gram-negative (*E. coli* K-12) and Gram-positive (*B. subtilis* 168) organism.

Figure 2. Disrupting chemotaxis proteins does not impair flagella assembly. Brucella broth cultures of wild-type NCTC11168 and the chemotaxis gene mutants and complemented strains were grown overnight at 37°C in microaerobic conditions. Cell were mounted between a microscope slide and coverslip and freshly prepared Ryu stain added adjacent to the coverslip. After five minutes, areas where the Ryu stain had penetrated were photographed at ×100 magnification using a Nikon Coolpix 4500 digital camera. Montage images and scale bars were prepared using ImageJ. Scale bar = 2 microns. Pictures are representative examples of multiple cultures each examined.

Figure 3. Chemotaxis mutants show a significant reduction in chemotactic motility in soft agar. For each chemotaxis mutant, the mutant strain was inoculated into 0.4% agar with the wildtype strain. Halo formation was measured after 24 and 48 hours and halo area expressed as the percentage of the wildtype halo for the same plate. Raw mean area of WT was 293.2 ± 15.52 and 1230 ± 63.69 mm^2 (24 and 48 hrs). Results are the mean from at least three biological replicates and error bars show standard deviation. An asterisk denotes statistically significant results, based on a one-sample *t*-test (comparison with wildtype) or a two-tailed Mann-Whitney test (*$p < 0.05$, **$p < 0.01$).

Figure 4. The *cheY* mutants show a 'catherine wheel' swimming phenotype consisting of repeated clockwise swimming. Following 6 – 7 hours growth at 37°C in microaerobic conditions, movies of swimming cells (a, wildtype; b, *cheY*; c, *cheY* +*cheY*; d, *cheY* +*cheY*^{D53A}; e, *cheY* +*cheY*^{D7A}; f, *cheY* +*cheA-Y*) were recorded at ×100 magnification using a light microscope and attached Nikon

683 camera. Individual cells were tracked using the Manual Tracking ImageJ plug-in and swimming
684 trajectories plotted using the Chemotaxis and Migration Tool (Ibidi).
685
686 **Figure 5.** Expressing a second copy of *cj0350* encoding a putative CheX homolog decreases
687 swarming motility. a) Chemotactic motility. Each strain was inoculated into 0.4% agar with the
688 wild-type strain. Halo formation was measured after 24 and 48 hours and halo area expressed as the
689 percentage of the wild-type halo for the same plate. Results are the mean from at least three
690 biological replicates and error bars show standard deviation. b) Tube Taxis. Assays were monitored
691 over 72 hours at 37°C and the dye front measured after 24, 48, and 72 hours. Migration was
692 calculated as a percentage of the wild-type used in the same assay. Results are the mean from at
693 least three biological replicates and error bars show standard deviation. c. Representative swarm
694 plate and tube taxis assays showing the WT +*cheX* phenotype. d. WT +*cheX* morphology shown
695 using scanning electron microscopy and Ryu staining. SEM scale bar = 1 micron, Ryu staining
696 scale bar = 2 microns.
697
698 **Figure 6.** Chemotaxis is required for biofilm formation at the air-media interface. Static cultures of
699 each strain were grown in the presence of a sterile glass slide, as shown in the cartoon on the right
700 (37°C, microaerobic, 48 hrs). Glass slides were removed and stained with 1% crystal violet. CV-
701 stained biofilm was detected using a GenePix microarray scanner employing both 635 and 532 nm
702 lasers. An asterisk shows the position of the air-media interface. Three independent biological
703 repeats are shown for each strain.
704

SUPPLEMENTARY INFORMATION

Supplementary figures

Figure S1. Chemotaxis mutants do not show impaired growth in Brucella media in microaerobic conditions.

Figure S2. Chemotaxis mutants show a significant reduction in migration in an energy and redox gradient.

Figure S3. RT-PCR analysis of chemotaxis gene expression in wildtype and mutant strains.

Figure S4. Strains containing two copies of chemotaxis genes have altered swarming and migration in taxis tubes.

Figure S5. *C. jejuni* CheY and CheA-Y share 58% similarity and contain the conserved acid pocket and aspartic acid active site residues.

Figure S6. The biofilm phenotype of the *che* mutants is linked to shedding of cells from the biofilm and the ability to swim to the air-media interface.

Supplementary Tables

Table S1. Oligonucleotide primers used in this study.

Table S2. Plasmids used in this study.

Other supplementary information

Supplementary Movie 1. Swimming behaviour of the *C. jejuni cheY* mutant.

Available via FigShare, doi: 10.15126/surreydata.7530881

Supplementary Movie 2. Swimming behaviour of the *C. jejuni* WT +*cj0350* (*cheX*) strain.

Available via FigShare, doi: 10.15126/surreydata.7530884

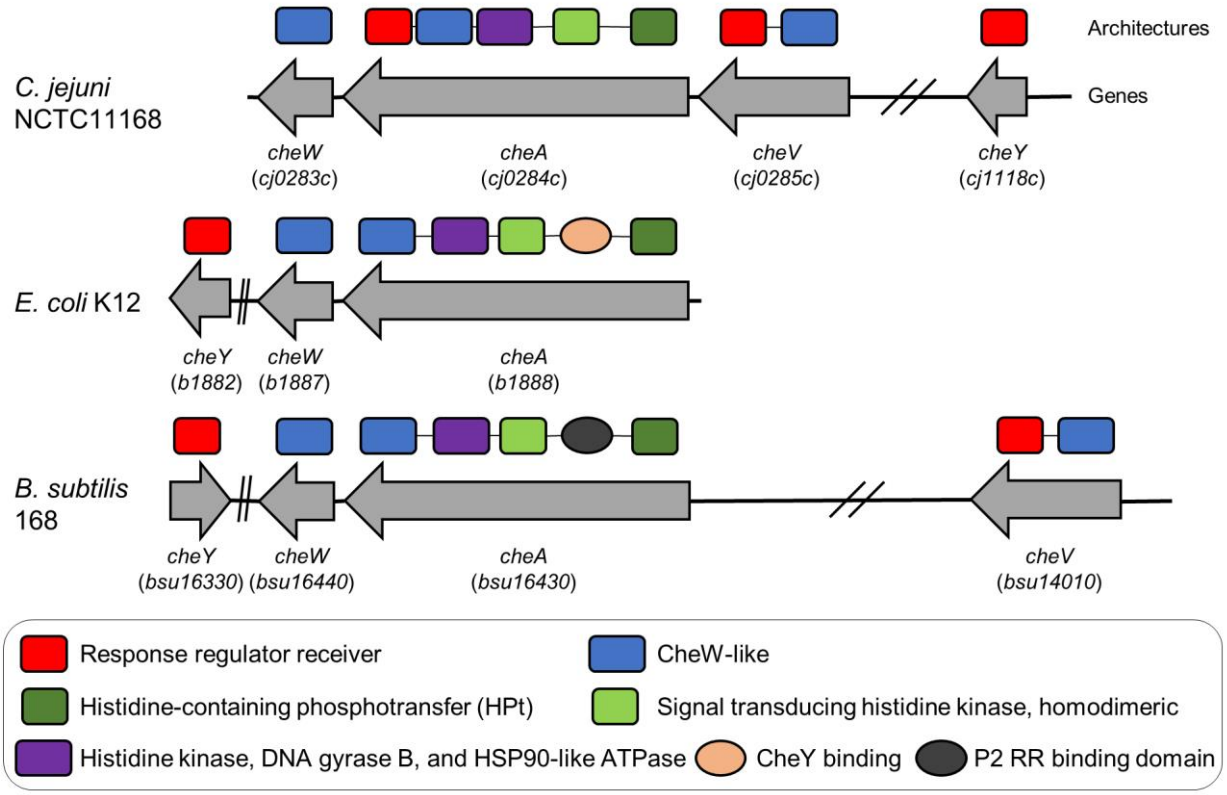

Figure 1. Architecture of the core CheV-A-W-Y chemotaxis system in *C. jejuni* compared to a model Gram-negative (*E. coli* K-12) and Gram-positive (*B. subtilis* 168) organism.

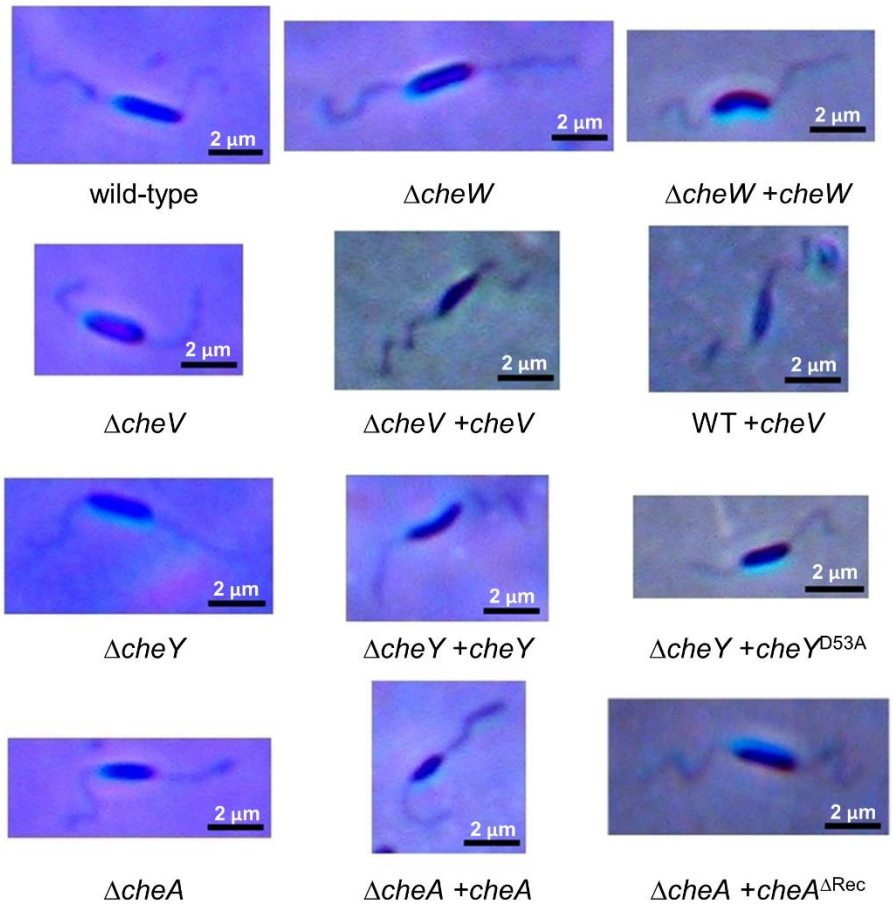

Figure 2. Disrupting chemotaxis proteins does not impair flagella assembly. Brucella broth cultures were grown overnight at 37°C in microaerobic conditions. Cell were mounted between a microscope slide and coverslip and freshly prepared Ryu stain added adjacent to the coverslip. After five minutes, areas where the Ryu stain had penetrated were photographed at ×100 magnification using a Nikon Coolpix 4500 digital camera. Montage images and scale bars were prepared using ImageJ. Scale bar = 2 microns.

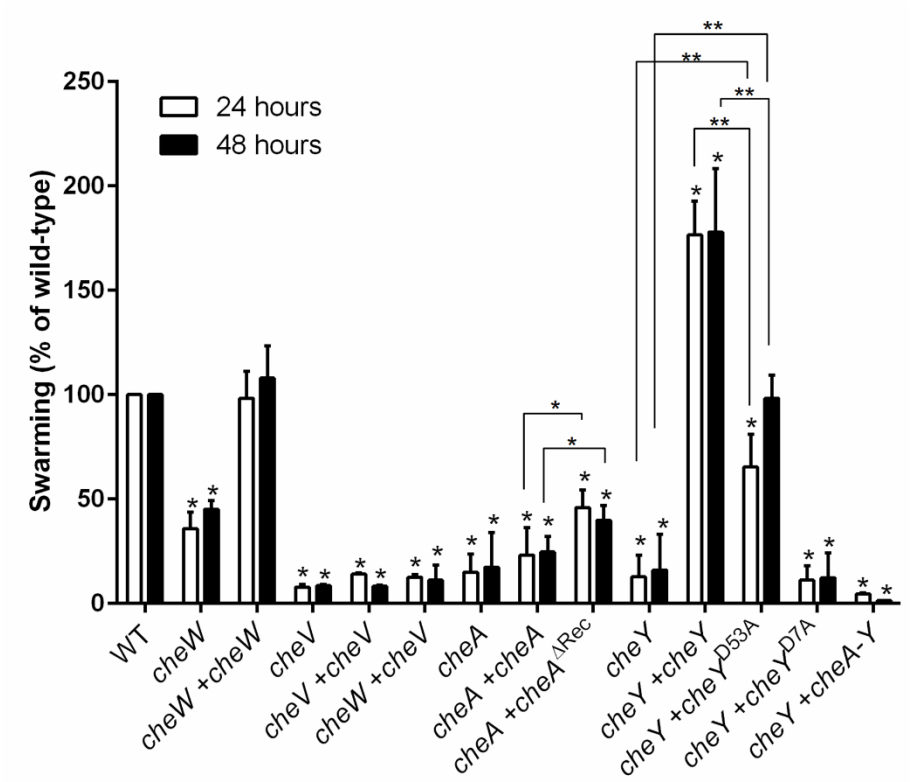

Figure 3. Chemotaxis mutants show a significant reduction in chemotactic motility in soft agar. For each chemotaxis mutant, the mutant strain was inoculated into 0.4% agar with the wildtype strain. Halo formation was measured after 24 and 48 hours and halo area expressed as the percentage of the wildtype halo for the same plate. Raw mean area of WT was 293.2 ± 15.52 and 1230 ± 63.69 mm^2 (24 and 48 hrs). Results are the mean from at least three biological replicates and error bars show standard deviation. An asterisk denotes statistically significant results, based on a one-sample *t*-test (comparison with wildtype) or a two-tailed Mann-Whitney test (*$p < 0.05$, **$p < 0.01$).

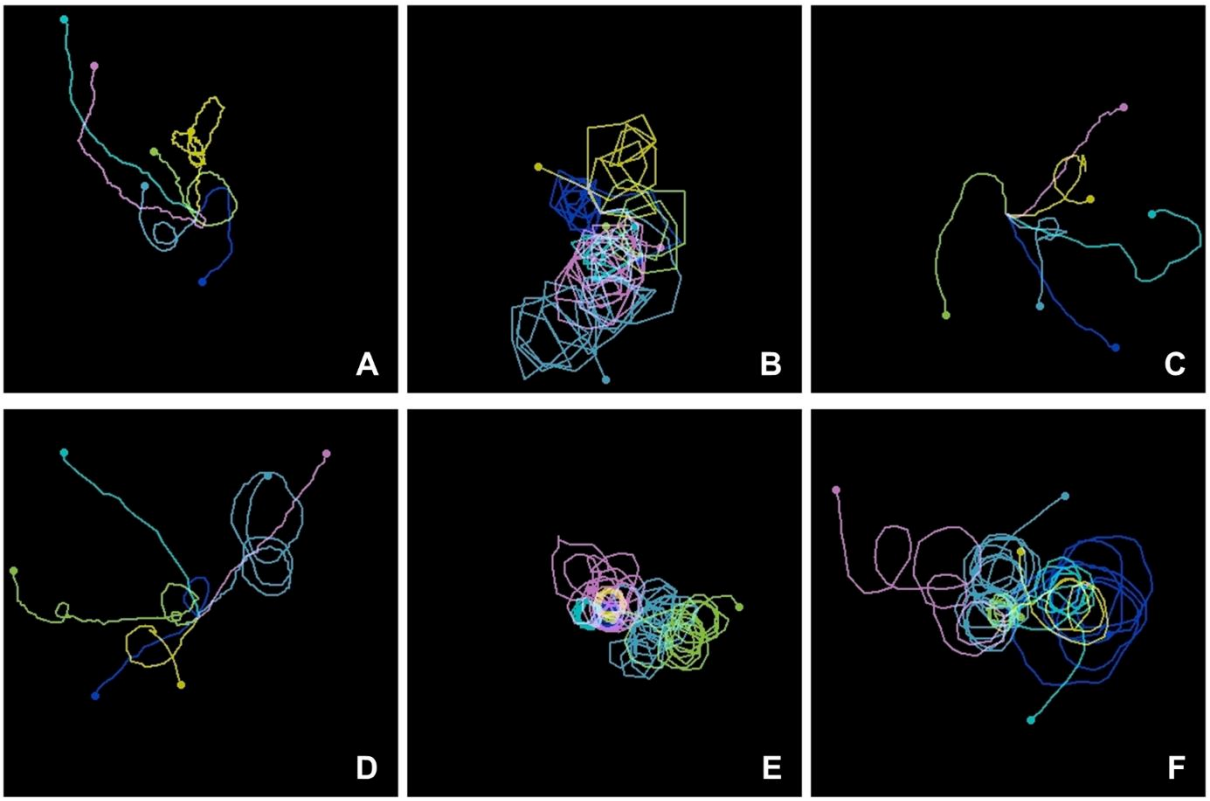

Figure 4. The *cheY* mutants show a 'catherine wheel' swimming phenotype consisting of repeated clockwise swimming. Following 6 – 7 hours growth at 37°C in microaerobic conditions, movies of swimming cells (a, wildtype; b, *cheY*; c, *cheY* +*cheY*; d, *cheY* +*cheY*^{D53A}; e, *cheY* +*cheY*^{D7A}; f, *cheY* +*cheA-Y*) were recorded at ×100 magnification using a light microscope and attached Nikon camera. Individual cells were tracked using the Manual Tracking ImageJ plug-in and swimming trajectories plotted using the Chemotaxis and Migration Tool (Ibidi).

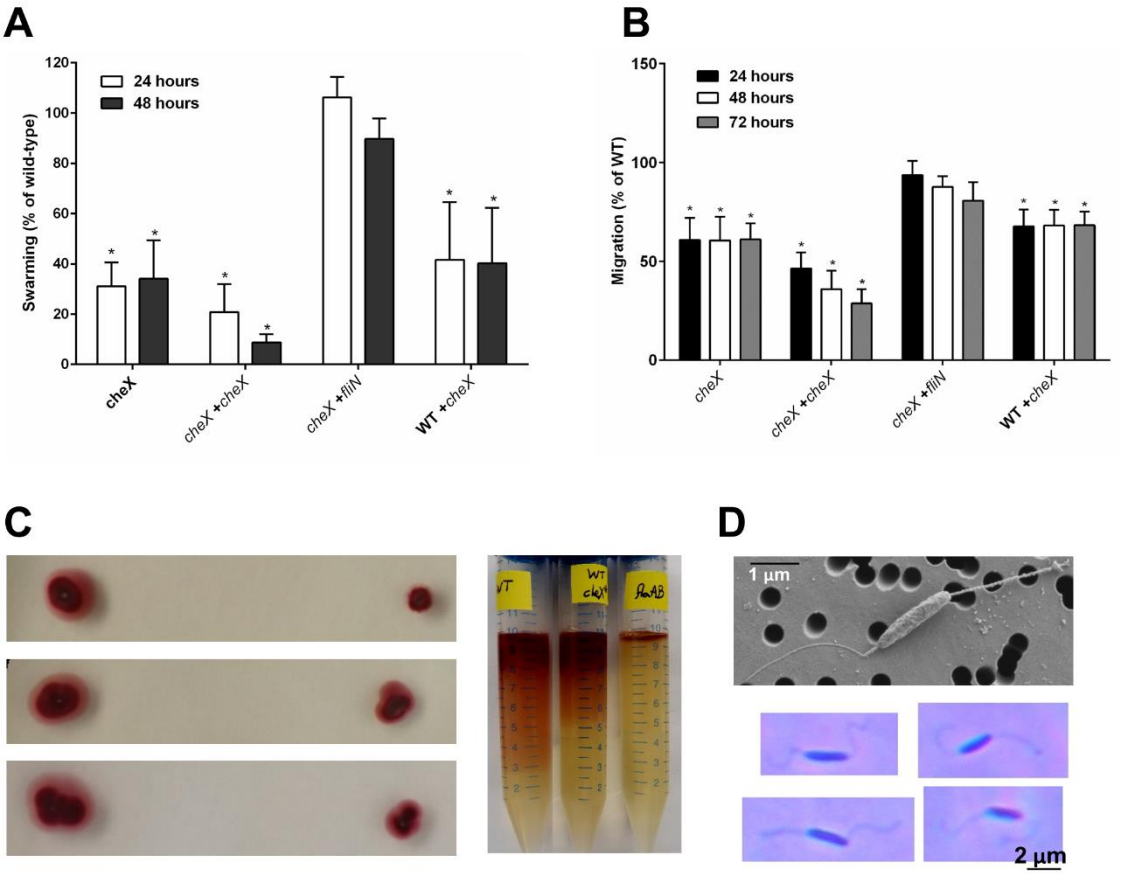

Figure 5. Expressing a second copy of *cj0350* encoding a putative CheX homolog decreases swarming motility. a) Chemotactic motility. Each strain was inoculated into 0.4% agar with the wild-type strain. Halo formation was measured after 24 and 48 hours and halo area expressed as the percentage of the wild-type halo for the same plate. Results are the mean from at least three biological replicates and error bars show standard deviation. b) Tube Taxis. Assays were monitored over 72 hours at 37°C and the dye front measured after 24, 48, and 72 hours. Migration was calculated as a percentage of the wild-type used in the same assay. Results are the mean from at least three biological replicates and error bars show standard deviation. c. Representative swarm plate and tube taxis assays showing the WT +*cheX* phenotype. d. WT +*cheX* morphology shown using scanning electron microscopy and Ryu staining. SEM scale bar = 1 micron, Ryu staining scale bar = 2 microns.

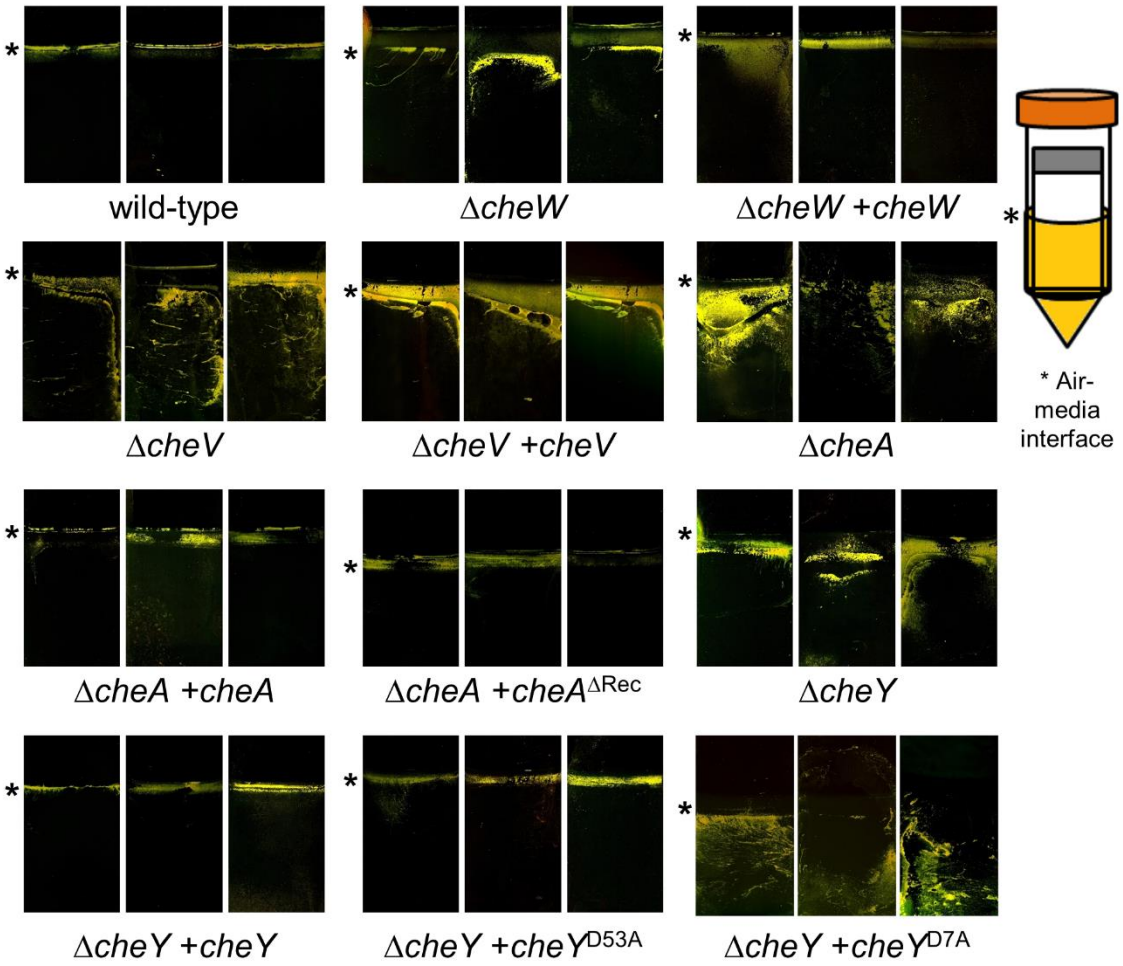

Figure 6. Chemotaxis is required for robust biofilm formation at the air-media interface. Static cultures of each strain were grown in the presence of a sterile glass slide, as shown in the cartoon on the right (37°C, microaerobic, 48 hrs). Glass slides were removed and stained with 1% crystal violet. CV-stained biofilm was detected using a GenePix microarray scanner employing both 635 and 532 nm lasers. An asterisk shows the position of the air-media interface. Three independent biological repeats are shown for each strain.